Received: 6 October 2022 | Accepted: 8 November 2022

DOI: 10.1002/pamm.202200098

Solving phase-field fracture problems in the tensor train format

Lennart Risthaus[1,*] and **Matti Schneider**[1]

[1] Karlsruhe Institute of Technology (KIT), Institute of Engineering Mechanics (ITM)

Phase-field models for the quasi-static simulation of brittle fracture where the crack is approximated by a damage phase-field are limited by the necessary memory and computation time. In this contribution, we study the applicability of low-rank methods to phase-field fracture models, specifically the tensor train (TT) format. To this end, we investigate the low-rank structure of the crack phase-field. Additionally, we present an implementation of an alternating minimization scheme to solve the coupled displacement and damage problem in the TT format. We show the evolution of the TT ranks of the displacement and damage fields for a specific example.

1 Introduction

1.1 State of the art

Based on the fundamental work of Griffith [1] and Francfort-Marigo [2], phase-field damage models [3, 4] approximate the nucleation and evolution of a crack in each time step by minimizing a functional consisting of the sum of the stored elastic energy and the crack surface energy. In phase-field damage models, the crack surface in a domain $Y = [0, L] \times [0, L]$ is approximated by a continuous phase-field variable $d : Y \to \mathbb{R}_{\geq 0}$. The width of the approximated crack is characterized by the length scale parameter η. For $\eta \to 0$, sharp cracks are recovered [4]. Besides finite elements, the elastic problem can be discretized using finite volumes [5] or finite differences [6]. For both approaches, sufficiently many degrees of freedom must be distributed across the crack, rendering a fine resolution imperative. Alas, the computational effort increases significantly for higher resolutions. As a potential remedy, we investigate the use of a low-rank method, specifically the tensor train (TT) format, an approach that has been shown to be efficient for other phase field problems [7], allowing for a finer resolution of the domain. The TT format was introduced by Oseledets [8, 9] to allow for the approximation of high-dimensional arrays by representing the array as a *train* of three-dimensional so-called TT cores. The TT format comes with a numerically stable algorithm for approximating full arrays and allows for algebraic operations without going back to the full representation. However, these algebraic operations increase the TT ranks. Therefore, specific linear solvers were proposed [10, 11] by optimizing the TT cores individually. An extension of the TT format, called the quantics tensor train (QTT) format was proposed by Khoromskij [12] to apply the TT format to low-dimensional problems. Using the QTT format, finite difference operators like the gradient or Laplacian admit efficient representations [13]. Vondřejc et al. [14] report an application of the tensor train format to linear elastic homogenization [14].

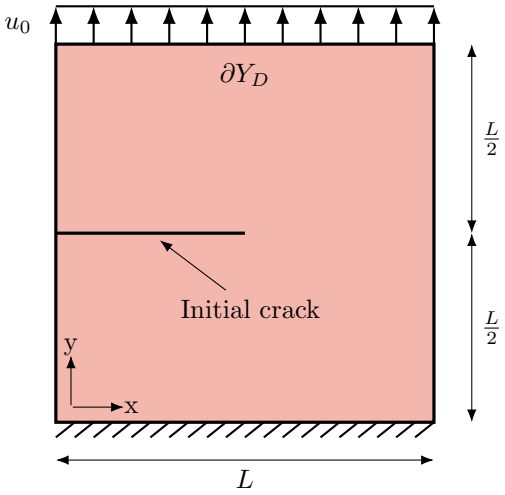

Fig. 1: Mode I crack with displacement boundary condition.

1.2 Contributions

We study the TT-rank structure of the damage phase-field approach by solving the problem in the QTT format. In sections 2 and 3, we provide necessary material concerning the theory of phase-field damage and the tensor train format, respectively. In section 4, we investigate the TT-ranks of the approximation of a *perfect* crack.

Then, in section 5, we investigate our approach to solving a phase-field fracture problem using an alternating minimization scheme [15] and the formulation of the damage and displacement sub-problems in the QTT format. We show that the damage field for the perfect crack possesses low QTT rank, whereas the damage field for a progressing crack does not. Additionally, we show that the displacement fields do not have low QTT ranks.

* Corresponding author: e-mail lennart.risthaus@kit.edu, phone +49 721 608 48781

2 Phase-field fracture

The phase-field fracture approach is based on the coupled minimization of a specific energy functional ψ w.r.t. the displacement u and the damage field d. In a two-dimensional setting, for a displacement field $u : Y \to \mathbb{R}^2$ and an associated strain $\varepsilon = \nabla^s u : Y \to \mathrm{Sym}(2)$ we split the elastic energy into two parts

$$\psi(\varepsilon, d) = g(d)\psi^+(\varepsilon) + \psi^-(\varepsilon). \tag{1}$$

More precisely, we use the energy split by Amor et al. [16]

$$\psi^+(\varepsilon) = \frac{\kappa_0}{2}\langle \mathrm{tr}(\varepsilon)\rangle_+^2 + \mu_0 \left(\varepsilon - \frac{1}{2}\mathrm{tr}(\varepsilon) I\right)^2 \quad \text{and} \tag{2}$$

$$\psi^-(\varepsilon) = \frac{\kappa_0}{2}\langle \mathrm{tr}(\varepsilon)\rangle_-^2, \tag{3}$$

where the negative part $\psi^-(\varepsilon, d)$ corresponds to the compression part of the deformation. The degradation function

$$g(d) = (1-\kappa)d^2 + \kappa \tag{4}$$

– using the residual stiffness factor $0 < \kappa \ll 1$ to ensure numerical stability [4] – controls the reduction of the stiffness by the damage d. We apply a pseudo-time-dependent displacement loading on the boundary $u_0 : [t_0, t_1] \times \partial Y_D \to \mathbb{R}^2$, see Fig 1. The quasi-static evolution of the damage field d is governed by the equation

$$(1 + f_\psi)d - 4\eta^2 \Delta d = f_\psi, \tag{5}$$

where the term f_ψ at time τ is determined by

$$f_\psi = \frac{4\eta}{G_c}(1-\kappa) \sup_{t_0 \le \tau \le t_1} \psi^+(\varepsilon) \tag{6}$$

with the critical energy release rate G_c, leading to a non-variational problem [4]. By taking the supremum of the energy $\psi^+(\varepsilon)$, we ensure the entire history of the elastic energy is accounted for and ensure a irreversibility of the crack opening [4]. Notice that only the positive (non-compression) part $\psi^+(\varepsilon)$ of the elastic energy drives the progress of the crack.

3 The tensor train format

To reduce the memory footprint of the numerical computations of phase-field fracture, we use a compression method called the tensor train (TT) format [8]. The TT format is employed to handle high-dimensional array-like structures $\mathbf{T} \in \mathbb{R}^{n_1 \times n_2 \times \cdots \times n_p}$ with n_k entries on the k-th dimension. Provided $n_1 = n_2 = \cdots = n_p = n$ holds, exactly n^p array entries need to be stored. If the entries of the tensor $\mathbf{T}$ are not independent and the TT ranks are low, a significant reduction in memory use can be obtained by a compression using the TT format. A tensor $\mathbf{T}$ in the TT format consists of a chain of so-called TT cores G_i which are three-dimensional arrays and which are linked by the auxiliary indices α_i, each ranging from 1 to the individual TT ranks r_i. The individual entries of the array $\mathbf{T}$ can be retrieved via a contraction over the auxiliary indices

$$T_{i_1,i_2,\ldots,i_p} \approx \sum_{\alpha_1,\alpha_2,\ldots,\alpha_{p+1}=1}^{r_1,r_2,\ldots,r_{p+1}} G_1(\alpha_1, i_1, \alpha_2)\, G_2(\alpha_2, i_2, \alpha_3) \ldots G_p(\alpha_p, i_p, \alpha_{p+1}), \tag{7}$$

where $r_1 = r_{p+1} = 1$. A quasi-optimal approximation in the Frobenius norm with a-priori accuracy of the array $\mathbf{T}$ can be found using an algorithm based on the Singular Value Decomposition [8]. Linear algebra operations, like addition, matrix-vector multiplication as well as the Kronecker product can be performed directly on arrays in the TT format, with the drawback that these operations, in general, increase the QTT rank of the result. Linear solvers are available that minimize each TT core individually [10, 11]. The TT format performs best for the compression of rather high-dimensional arrays, but evidently the dimension of fields for phase-field fracture is three at most. Therefore, we use an adaptation of the TT format, the quantics tensor train (QTT) format [12], where low-dimensional arrays are first reinterpreted as a high-dimensional array with two entries per dimension and are subsequently compressed using the TT decomposition. For a fixed QTT rank, the memory required grows only logarithmically in the number of entries N of the original array. Using the QTT format, certain finite-difference operators, like the Laplace operator with a maximum QTT rank of four, can be represented with low QTT rank [13].

4 Cracks on the tensor train

4.1 The perfect crack

For an efficient evaluation of phase-field fracture using a tensor train approach, the QTT ranks of the underlying discretized damage field must remain reasonably low. The approximation of a fully developed crack through the two-dimensional domain Y is expressed analytically [4] as

$$d(x, y) = \mathrm{e}^{-|y-L/2|}.$$

This crack field is shown in Fig. 2. Discretized values of the exponential function admit an exact representation by a rank-2 QTT field [12]. Using a series of Kronecker products, we construct a fully developed, straight crack through a two-dimensional domain on a discrete grid of edge length $N = 2^p$ manually and analyze its QTT ranks. Fix the vectors $e_1 = [1, 0]^T$ and $l = [1, 1]^T$. The vector

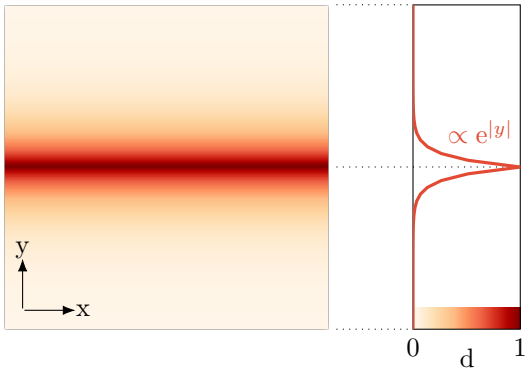

Fig. 2: An analytically constructed crack through a two-dimensional domain with a maximum QTT rank of two.

$$k_{\mathrm{top}} = e_1 \otimes \underbrace{l \otimes l \otimes \cdots \otimes l}_{p-1 \text{ times}} \quad \in \mathbb{R}^{4^p} \tag{8}$$

represents a field where the top half is one and the bottom half is zero when reshaped into a $2^p \times 2^p$ array. Employing the same approach, the complementary field k_{bottom} (where the bottom half is one) is constructed by exchanging e_1 for $e_2 = [0, 1]^T$. The field k_a with all ones is constructed by switching e_1 for l.

The Kronecker product for two QTT tensors equals a chaining of the two groups of QTT cores. The QTT representation of the vectors e_i and l by construction consists of a single core which is a reshape of the vectors themselves to the shape $[1, 2, 1]$. The (two) QTT ranks of this vector are one. Therefore, the $(p + 1)$ QTT ranks of both fields k_{top} and k_{bottom} are all one.

Using a Taylor series, we approximate the QTT cores g_k of the one-dimensional exponential function $m_{\alpha,s} = \exp(\alpha x - s)$ on a 2^p grid [12]. Let the k-th core

$$g_k = \begin{cases} \begin{bmatrix} 0 \\ \exp\left(\alpha \cdot 2^{p-k-1}\right) \end{bmatrix}, & k = p - 1 \\ \begin{bmatrix} \exp\left(\alpha \cdot s \cdot 2^{p-k-1}\right) \\ \exp\left(\alpha \cdot (1 + s) \cdot 2^{p-k-1}\right) \end{bmatrix}, & \text{otherwise,} \end{cases} \tag{9}$$

which is reshaped to $[1, 2, 1]$ to obtain the standard format of a rank-1 TT core. This results in a series of cores with rank one.

For QTT vectors of the same length, the pointwise (or Hadamard) product translates into a multiplication of the respective QTT ranks with the same index. Accordingly, taking the Hadamard product of either the top field k_{top} or the bottom field k_{bottom} with the exponential function $m_{\alpha,s}$ retains QTT ranks of all one. This product represents the projection of the exponential function to either half of the one-dimensional domain. When adding two QTT tensors, the respective QTT ranks with the same index sum up. We approximate the initial function $u(x, y) = \exp(-|y - N/2|)$ by

$$u_{1\mathrm{D}} = k_{\mathrm{top}} \otimes m_{1,-N/2+1} + k_{\mathrm{bottom}} \otimes m_{1,-N/2}. \tag{10}$$

As we noted previously, this sum raises the maximum QTT ranks of the field to two. Finally, to obtain the crack as a two-dimensional discrete field $u_{2\mathrm{D}}$, we perform a final Kronecker product as follows:

$$u_{2\mathrm{D}} = u_{1\mathrm{D}} \otimes k_a. \tag{11}$$

Ultimately, as the QTT ranks of the field k_a are all one, the perfect crack field has maximum QTT ranks of two. The maximum rank of the field is independent of the parameter p. Therefore, as the maximum rank is independent of d, the memory required for handling the field is only affected by the increase of QTT cores, which scales logarithmically with the edge length N.

4.2 Applying boundary conditions in the tensor train format

Accessing single entries of fields in the tensor train format increases the QTT ranks and is therefore costly. To solve the mechanical sub-problem, we use a projector-based application of the boundary conditions allowing us to access single entries once and then use TT matrix-vector products to apply the projectors. Accordingly, when using the degradation function (4) for the displacement sub-problem, the balance of linear momentum

$$0 = \nabla \cdot \sigma \tag{12}$$

may be transformed successively

$$0 = \nabla \cdot \left[g(d)\mu_0 \nabla^s u + g(d)\lambda_0 (\nabla \cdot u)\mathrm{I} \right], \tag{13}$$

$$0 = \nabla \cdot \left[g(d)\mu_0 \nabla^s + g(d)\lambda_0 (\nabla \cdot)\mathrm{I} \right] u, \tag{14}$$

$$0 = \underbrace{\nabla \cdot \left(\mathbb{C}(d) \nabla^s \right)}_{A} u, \tag{15}$$

$$0 = Au. \tag{16}$$

where $\mathbb{C}(d)$ denotes the damage-dependent stiffness tensor. By employing a projector-based split

$$u = \tilde{u} + u_D + u_N = \mathbb{P}^u_{\mathrm{S}} u + \mathbb{P}^u_{\mathrm{D}} u + \mathbb{P}^u_{\mathrm{N}} u \tag{17}$$

of the solution vector u into the values $\tilde{u}$ on the interior points $Y \setminus \partial Y$, the values u_D on the Dirichlet boundary ∂Y_D and the points u_N on the Neumann boundary ∂Y_N, we set up our system of equations. The projectors are related by

$$\mathbb{P}^u_S = 1 - \mathbb{P}^u_D - \mathbb{P}^u_N. \tag{18}$$

Then, the system of equations is

$$\left[\mathbb{P}^u_S A + \mathbb{P}^u_D + \mathbb{P}^u_N \left(\nabla \cdot n \right) \right] u = u_D, \tag{19}$$

which we then solve for u. This approach – even though we also solve for the "known unknowns" u_D – allows to bypass odd sizes for tensor fields which could occur otherwise (depending on the prescribed boundary conditions) as the QTT format works best with arrays with sizes multiples of two.

Analogously, for the damage field $d = \tilde{d} + d_D + d_N$, we employ a similar approach to handle the boundary conditions of the damage sub-problem

$$(1 + f_\psi)d - 4\eta^2 \Delta d = f_\psi \tag{20}$$

as follows:

$$\left[(1 - \mathbb{P}^d_D) \left[(1 - \mathbb{P}^d_N) \left(1 + \mathrm{diag}(f_\psi) \right) - 4\eta^2 \Delta \right] + \mathbb{P}^d_D \right] d = (1 - \mathbb{P}^d_D) \left[(1 - \mathbb{P}^d_N) f_\psi \right] + d_D. \tag{21}$$

Defining $\mathbb{P}^d_S = (1 - \mathbb{P}^d_D)(1 - \mathbb{P}^d_N) = 1 - \mathbb{P}^d_N - \mathbb{P}^d_D$, the system of equation for the damage field d becomes

$$\left[\mathbb{P}^d_S \left(1 + \mathrm{diag}(f_\psi) \right) - (1 - \mathbb{P}^d_D) 4\eta^2 \Delta + \mathbb{P}^d_D \right] d = \mathbb{P}^d_S f_\psi + d_D. \tag{22}$$

Empirically, all these projectors $\mathbb{P}$ possess a QTT rank of one, therefore they do not increase the ranks of the investigated fields.

5 Results

5.1 Setup

To solve the phase-field fracture problem in a QTT framework, we implemented a custom tensor train Python library [7] to use a finite difference discretization with all damage, displacement, strain, and stress fields as well as the operators in the QTT format. All simulations were performed on an Intel Core i7 octa-core processor with 64 GB of RAM. We used a Young's modulus of $\mathrm{E} = 210\,\mathrm{GPa}$ and Poisson's ratio of $\nu = 0.3$ for the linear elastic simulations. An energy release rate of $G_c = 2.7\,\mathrm{MPa/mm}$ and residual stiffness factor $\kappa = 10^{-6}$ were used for evaluating the phase-field. We investigate a mode I crack on a square geometry with a displacement boundary condition on the top of the geometry as shown in Fig. 1.

5.2 The crack tip position

By minimizing the crack surface density function of a crack at prescribed positions of the crack tip [4], we solve for the damage field using the QTT framework. This procedure enables us to analyze the QTT ranks of the damage field for cracks that have not yet fully developed.

On a regular square grid with Neumann boundary conditions on the edges of the grid, we solve the equation

$$d - \eta^2 \Delta d = 0$$

for the damage d to minimize the surface energy, where Δ denotes the Laplace operator and η stands for the crack length scale [4]. In Fig. 3, the maximum QTT ranks of the regularized crack field are displayed for various crack tip positions. The QTT ranks of the damage field remain consistently higher for all crack tip positions that do no lie in the vicinity of the domain boundary. Varying the crack length scale η does not significantly alter the maximum QTT ranks. When the crack tip is on the boundary of the domain and the fully developed crack state is reached, the QTT ranks are significantly lower – a result that is in accordance with the results from the previous section. As the ranks of the damage field are reasonably low, we want to turn our focus to the evaluation of the displacement field and strain field in the tensor train format.

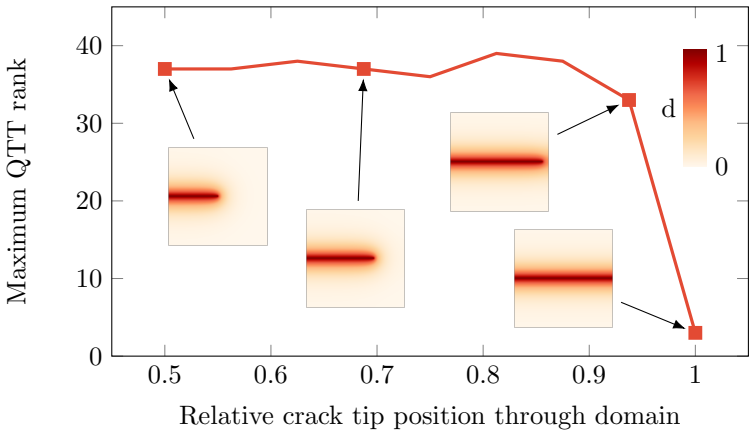

Fig. 3: Maximum QTT ranks of the damage field for various positions of the crack tip on a 256×256 grid and respective damage fields at selected positions.

5.3 The mechanical sub-problem

To get a first insight to the QTT ranks of the displacement and strain fields during the evaluation of phase-field fracture, we evaluate the regularized damage field as elaborated in section 4 and use this damage field to apply the degradation function (4) to the mechanical problem, where we use Dirichlet boundary conditions on the top and bottom boundary to prescribe a displacement and use Neumann boundary condition on the left and right boundary. The prescribed displacement u_0, applied at the top edge is scaled linearly with the crack tip position from 0 to $0.07L$. The resulting maximum QTT ranks as well as the respective displacement fields are shown in Fig. 4. We see that for the unloaded state, the QTT ranks of the displacement field are rather low, which is a result of the homogeneous nature of the unloaded displacement field. With the onset of loading, the maximum QTT ranks immediately rise to 64, the maximum value possible on a 64×64-grid.

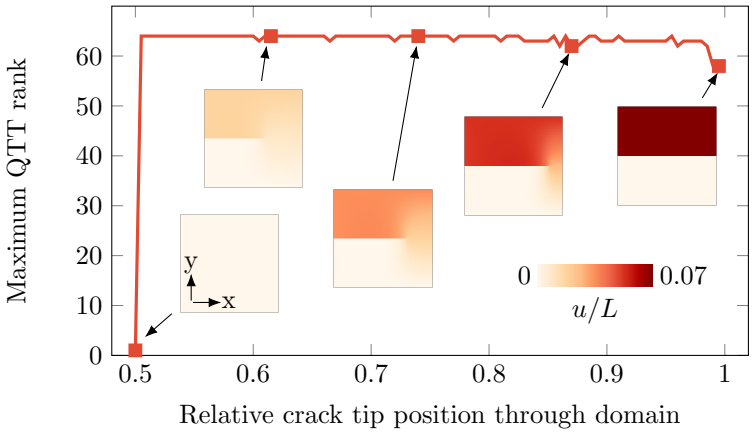

Fig. 4: Maximum QTT ranks of the displacement field for various positions of the crack tip on a 64×64 grid of edge length L and respective displacement fields in y-direction at selected positions for the uncoupled problem

5.4 Evaluation of the coupled phase-field fracture problem

Eventually, we evaluate a fully coupled alternating minimization [3, 15] of the elastic (1) and the phase-field (5) problem using the coupling outlined in section 2. After a total of 137 computation steps with a displacement increment of $7 \cdot 10^{-4}$ each, the crack tip has reached the right boundary of the domain. As we see on Fig. 5, after a single computation step, the maximum QTT ranks of the damage field reach a value of 64. After this first computation step, the ranks of the displacement field also reach the maximum value of 64. During the course of the crack progression, the maximum QTT ranks do not decrease anymore. In contrast to the uncoupled solution in Fig. 4, the damage field is less ordered. For a two-dimensional field, this means the field has full rank [8] suggesting that this problem appears not well suited for approximation using the TT format.
Compressing the displacement field to a lower maximum QTT rank leads to no convergence.

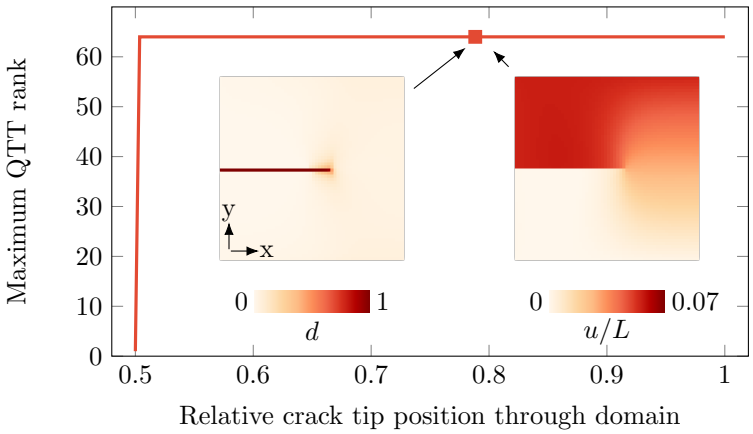

Fig. 5: Maximum QTT ranks for the ranks field for a fully coupled solution on a 64×64-grid as well as damage and displacement fields after 80 computation steps.

6 Conclusion

In this work, we introduced a novel TT low-rank approach to solve phase-field fracture problems. We showed that the perfect crack has low QTT ranks. In constrast, the displacement field has elevated ranks, diminishing the memory savings for storing the displacement field in the TT format and the ranks scaling with the resolution, negating the advantages of using the (Q)TT format. On the other hand, we showed that the operators in fact always possess low rank. The applicability of this approach to the fully coupled solution of phase-field fracture is further bottlenecked by the multiplication by the elastic energy, which does not have low QTT rank, and the complex application of material laws.

Acknowledgements Support by the Deutsche Forschungsgemeinschaft (DFG, German Research Foundation) - 418247895; 255730231 - is gratefully acknowledged. Open access funding enabled and organized by Projekt DEAL.

References

[1] A. A. Griffith and G. I. Taylor, Philosophical Transactions of the Royal Society of London. Series A, Containing Papers of a Mathematical or Physical Character **221**(582-593), 163–198 (1921).
[2] G. A. Francfort and J. J. Marigo, Journal of the Mechanics and Physics of Solids **46**(8), 1319–1342 (1998).
[3] B. Bourdin, G. Francfort, and J. J. Marigo, Journal of the Mechanics and Physics of Solids **48**(4), 797–826 (2000).
[4] C. Miehe, M. Hofacker, and F. Welschinger, Computer Methods in Applied Mechanics and Engineering **199**(45), 2765–2778 (2010).
[5] C. Dorn and M. Schneider, International Journal for Numerical Methods in Engineering **118**(11), 631–653 (2019).
[6] M. Schneider, F. Ospald, and M. Kabel, International Journal for Numerical Methods in Engineering **105**(9), 693–720 (2016).
[7] L. Risthaus and M. Schneider, Applied Numerical Mathematics **178**, 262–279 (2022).
[8] I. V. Oseledets, SIAM Journal on Matrix Analysis and Applications **31**(4), 2130–2145 (2009).
[9] S. R. White, Physical Review B **48**(14), 10345–10356 (1993).
[10] S. Holtz, T. Rohwedder, and R. Schneider, SIAM Journal on Scientific Computing **34**(2), A683–A713 (2012).
[11] I. V. Oseledets, Computational Methods in Applied Mathematics **11**(3), 382–393 (2011).
[12] B. N. Khoromskij, Constructive Approximation **34**(2), 257–280 (2011).
[13] V. A. Kazeev and B. N. Khoromskij, SIAM Journal on Matrix Analysis and Applications **33**(3), 742–758 (2012).
[14] J. Vondřejc, D. Liu, M. Ladecký, and H. G. Matthies, Computer Methods in Applied Mechanics and Engineering **364**, 1–25 (2020).
[15] F. Ernesti, M. Schneider, and T. Böhlke, Computer Methods in Applied Mechanics and Engineering **363**, 112793 (2020).
[16] H. Amor, J. J. Marigo, and C. Maurini, Journal of the Mechanics and Physics of Solids **57**(8), 1209–1229 (2009).